



THE UNIVERSITY *of* EDINBURGH

Edinburgh Research Explorer

The structure of human thyroglobulin

Citation for published version:

Coscia, F, Taler-Verčič, A, Chang, VT, Sinn, L, O'Reilly, FJ, Izoré, T, Renko, M, Berger, I, Rappsilber, J, Turk, D & Löwe, J 2020, 'The structure of human thyroglobulin', *Nature*, vol. 578, no. 7796, pp. 627-630. <https://doi.org/10.1038/s41586-020-1995-4>

Digital Object Identifier (DOI):

[10.1038/s41586-020-1995-4](https://doi.org/10.1038/s41586-020-1995-4)

Link:

[Link to publication record in Edinburgh Research Explorer](#)

Document Version:

Peer reviewed version

Published In:

Nature

General rights

Copyright for the publications made accessible via the Edinburgh Research Explorer is retained by the author(s) and / or other copyright owners and it is a condition of accessing these publications that users recognise and abide by the legal requirements associated with these rights.

Take down policy

The University of Edinburgh has made every reasonable effort to ensure that Edinburgh Research Explorer content complies with UK legislation. If you believe that the public display of this file breaches copyright please contact openaccess@ed.ac.uk providing details, and we will remove access to the work immediately and investigate your claim.



1

2 **The structure of human thyroglobulin-2019-07-11446A**

3

4 Francesca Coscia¹, Ajda Taler-Verčič^{2,3}, Veronica T. Chang¹, Ludwig Sinn⁴,

5 Francis J. O'Reilly⁴, Thierry Izoré¹, Miha Renko², Imre Berger⁶,

6 Juri Rappsilber^{4,5}, Dušan Turk^{2,3,*}, Jan Löwe^{1,*}

7

8 ¹: MRC Laboratory of Molecular Biology, Cambridge CB2 0QH, UK

9 ²: Jožef Stefan Institute, 1000 Ljubljana, Slovenia

10 ³: Centre of Excellence for Integrated Approaches in Chemistry and Biology of Proteins,
11 1000 Ljubljana, Slovenia

12 ⁴: Institute of Biotechnology, Technische Universität Berlin, 13355 Berlin, Germany

13 ⁵: Wellcome Centre for Cell Biology, University of Edinburgh, Edinburgh EH9 3BF, UK

14 ⁶: University of Bristol, Bristol, BS8 1TD, UK

15

16 * shared corresponding authors:

17 Jan Löwe, MRC Laboratory of Molecular Biology, Francis Crick Avenue, Cambridge CB2
18 0QH, UK, +44 (0)1223 267064, jyl@mrc-lmb.cam.ac.uk

19 Dušan Turk, Jožef Stefan Institute, Jamova 39, 1000 Ljubljana, Slovenia, +386 (0) 1 477
20 3857, dusan.turk@ijs.si

21 Keywords: thyroglobulin; thyroxine; T3; T4; thyroid hormone; tyrosine iodination;
22 cryo-EM

23 **SUMMARY**

24 Thyroglobulin is the protein precursor of thyroid hormones, which are essential for
25 growth, development and control of metabolism in vertebrates^{1,2}. Hormone synthesis
26 from thyroglobulin (TG) occurs in the thyroid gland via the iodination and coupling of
27 pairs of tyrosines and is completed by TG proteolysis³. Tyrosine proximity within TG is
28 thought to enable the coupling reaction but hormonogenic tyrosines have not been
29 clearly identified and the lack of a three-dimensional structure of TG has prevented
30 mechanistic understanding⁴. Here we present the structure of full-length human
31 thyroglobulin at ~ 3.5 Å resolution determined by electron cryomicroscopy (cryo-EM).
32 We identified all hormonogenic tyrosine pairs in the structure and verified them via
33 site-directed mutagenesis and *in vitro* hormone production assays using human TG
34 expressed in HEK cells. Analysis revealed that proximity, flexibility and solvent
35 exposure of the tyrosines are the key characteristics of hormonogenic sites.
36 Transferring the reaction sites from TG to an engineered tyrosine donor-acceptor pair
37 in the unrelated bacterial maltose binding protein (MBP) yielded hormone production
38 with efficiency comparable to TG. Our study provides a framework to further
39 understand the production and regulation of thyroid hormones.

40 **MAIN**

41 Tetraiodothyronine (thyroxine, T4) and triiodothyronine (T3) are iodine-containing
42 thyroid hormones (TH) that regulate metabolism and many other fundamental
43 processes in vertebrates^{1,5}. T4 and smaller amounts of T3 are found in the bloodstream
44 of healthy humans³, whereas suboptimal levels of TH have dramatic consequences for
45 heart rate, brain function and foetal development. Approximately 5% of the world's
46 human population suffer from thyroid diseases, but the molecular events behind TH
47 synthesis are yet to be completely understood⁶.

48 TH synthesis is stimulated by TSH (thyroid stimulating hormone), itself produced in
49 pituitary gland, to occur in the thyroid from the protein precursor thyroglobulin (TG).
50 Iodide (I⁻) is accumulated in the thyroid both in the cytoplasm and lumen of thyroid
51 follicular cells (colloid), into which TG is secreted in high amounts^{2,7}. Two apical
52 membrane enzymes dual oxidases (DUOX, producing H₂O₂) and thyroid peroxidase
53 (TPO, oxidising iodide) allow the extracellular iodination of tyrosine residues within the
54 TG protein substrate^{3,8}. TG, a protein dimer of 600 kDa, has an unusually high number
55 of ~ 60 disulfide bonds per monomer and 17 glycosylation sites, which confer
56 remarkable stability and solubility to the protein^{1,2,9}. Of ~30 iodinated tyrosines in TG
57 per monomer (out of 66), only a small number are hormonogenic, i.e. are a substrate for
58 TH formation. In the hormonogenic sites, after iodination, the aromatic ring of a donor
59 di- (or mono-) iodo-tyrosine is transferred to a proximal acceptor di-iodo-tyrosine,
60 thereby forming T4 (or T3) hormone, still connected to the polypeptide backbone, while
61 leaving a dehydroalanine at the donor position¹⁰. After endocytosis from the colloid to
62 cytoplasmic lysosomes, TG is proteolysed in follicular cells and releases free TH
63 (Extended Data Figure 1)^{11,3}. Furthermore, a thyroid dehalogenase (Dehal1) recycles
64 iodide stored in non-homonogenic iodotyrosines of TG¹².

65 Mass spectrometry analyses of thyroid-extracted TG have identified four or more
66 acceptor tyrosines, but the position of the donors has remained unclear¹³.

67 We recombinantly produced full-length non-iodinated human TG in HEK293T cells
68 (rTG)¹⁴. rTG appears to be indistinguishable by SDS-PAGE and cryo-EM from
69 endogenous TG purified from thyroid glands of goitrous patients (eTG), which is partly
70 iodinated (Extended Data Figure 2 a-c). In cryo-EM, TG has a bilobed shape with

71 average dimensions of 120 x 235 Å, which correlate well with previously reported
72 negative staining EM data¹⁵. We collected cryo-EM datasets for both rTG and eTG and
73 obtained very similar reconstructions at the resolution of ~3.5 Å (Extended Data Figure
74 2 d-g, Extended Data Table 1). The initial maps obtained by imposing C2 symmetry
75 showed local resolutions ranging from ~3 to ~6 Å. Symmetry expansion and focussed
76 refinements improved the quality of the peripheral regions (Extended Data Figure 2 e).
77 Using a combination of *de novo* and homology modelling we built a TG atomic model
78 covering 93% of its 2749 amino acids, with variable local quality (Extended Data Figure
79 3).

80 TG's sequence is dominated by a number of cysteine rich domains, which have been
81 named type 1, 2 and 3 thyroglobulin-like repeats (Figure 1a)^{16,17,18}. TG-repeats are
82 spaced by linker domains and connected to a C-terminal choline esterase-like domain
83 (ChEL). Following the domain arrangement in the context of TG's 3D structure, we
84 defined five TG regions: NTD (N-terminal domain), Core, Flap, Arm and CTD (C-terminal
85 domain), as indicated in Figures 1a-b. TG's dimer interface is very large at 29,350 Å²
86 (Figures 1c-e, Supplementary Video 1). In the TG monomer, the globular NTD is
87 connected to the Core region via a linker (residues 610-620), crossing the central dimer
88 interface and it is partially flexible (Extended Data Figure 2f). The Core contains two
89 triplets of type-1 repeats (domain H with a very large insertion), separated by domain I,
90 located near the C2 axis. The Core is then connected to the Flap region, which is
91 composed of two Ig-like domains, M and N. The Flap extends along the minor axis of the
92 molecule with the M domain protruding at the opposite side of the NTD and folding
93 back onto the Arm region. The Arm consists of a rod-shaped arrangement formed by
94 concatenated type-2 TG repeats with a laminin-like fold and by a single type-1 repeat P.
95 This is followed by a series of type-3 TG repeats, tightly docking onto each other in an
96 arc towards the direction of the C2 axis. The Arm is linked to the CTD region,
97 corresponding to the dimeric ChEL domain, located near the C2 axis. Overall, TG's
98 structure appears entangled and revolves around the central ChEL dimer that interacts
99 with different regions of the Arm and the Core of the same chain and, via the E domain,
100 with the NTD of the other chain. Due to the intertwined nature of the dimer, the NTD
101 interacts with all regions of the other subunit of the dimer. To validate the complex TG
102 architecture, we used crosslinking mass spectrometry and found that the predicted

103 inter- and intra-molecular links from our atomic model are in excellent agreement with
104 experimental crosslinks (Extended Data Figure 4). For example, we detected long-range
105 crosslinks that are consistent with the TG fold where the NTD crosses the ChEL dimer
106 interface: 539-2524, the N-terminus with 178 and the Arm region 1987-1990 (Extended
107 Data Figure 4d-f). Most of TG's disulfide bonds show clear EM density in our maps
108 (Extended Data Figure 5a) and we found no inter-subunit disulfide bonds, in agreement
109 with previous observations that TG is a non-covalent dimer¹⁹. We resolved 12
110 previously predicted N-linked GlcNac in our maps, and four that had not been identified,
111 at N110, N484, N1869 and N2122²⁰ (Extended Data Table 3). Some glycans are partially
112 buried and are resistant to treatment with deglycosylases, as shown by EM. Notably, the
113 glycans linked to N2013 mediate the contact between the NTD and CTD and might
114 contribute to the dimer stability (Extended Data Figure 5b & f, Supplementary Video 1).

115 We inspected our structure within a 15 Å radius of the reported acceptor tyrosines
116 (designated Sites A-D)²¹ and identified putative donor tyrosines (Figure 2a). Acceptor
117 Y24 (partially disordered) at Site A appears to have two possible donor partners Y234
118 and Y149 (donor 1 and donor 2). In Site B the acceptor Y2573 pairs with donor Y2540;
119 At Site C, Y2766, not resolved in our maps, probably acts both as donor and acceptor
120 across the C2 dimer axis¹⁹. In Site D the acceptor Y1310 pairs with Y108 of the other
121 subunit (Figure 2a). Therefore, TG likely contains four homonogenic acceptor tyrosines
122 and five donor tyrosines. We verified this by comparing the amount of TH obtained
123 from unmodified rTG and rTG variants where acceptor or donor tyrosines were
124 mutated to phenylalanines, abolishing hormone formation. TH synthesis was performed
125 by rTG *in vitro* iodination, and the T4 or T3 concentrations were measured by adapting
126 a commercial ELISA assay (Extended Data Figure 6)^{22,23}. Using our reaction conditions,
127 we could only detect significant production of T4, but not of T3 (Extended Data Figure
128 6f-g). We used lactoperoxidase (LPO) in all other reactions, since it showed the same
129 activity as TPO in our assay⁸. As shown in Figure 2c, when we mutated all acceptors
130 (Y24, Y2573, Y2766 and Y1310)^{21,13} we observed no T4 synthesis, demonstrating that
131 there are no more than four significant homonogenic sites in TG. A residual activity,
132 corresponding to about a third of unmodified rTG activity, was detected by mutating all
133 but one of the proposed donors for Site A: those at Sites B, C and D (Y2540, Y2766 and
134 Y108), and either donor 1 or donor 2 at Site A (Y234 and Y149). When all five proposed

135 donors were mutated, no significant T4 formation could be detected, confirming that
136 Site A indeed has two donor tyrosines: Y234 and Y149. We also mutated four exposed
137 tyrosines (4eY), suggested as being important for hormonogenesis^{21,24} and obtained the
138 same activity as for un-mutated rTG. Therefore, at least under the conditions used, we
139 unequivocally determined and validated the complete set of tyrosines involved in the
140 four TG hormonogenic Sites A, B, C and D. The uniqueness of these tyrosine pairs is
141 corroborated by the analysis of all tyrosine pairs at less than 15 Å distance from each
142 other, calculated from the TG structure (Extended Data Figure 7 a & c). We found that
143 only the tyrosines at TG's hormonogenic sites appear sufficiently close and exposed to
144 permit T4 synthesis. Within the overall TG structure, Site A is located in the NTD, Site B
145 in the CTD, Site C is at the C-terminus across the C2 dimer interface and Site D bridges
146 the NTD and Flap (M domain) of the other subunit in the dimer (Figure 2b).

147 Furthermore, we showed that all acceptor mutants with one hormonogenic site active at
148 a time (Figure 3a) contribute to hormone formation and the sum of the concentrations
149 measured individually recapitulates the total T4 amount produced by unmodified rTG.
150 We conclude that TG synthesises seven molecules of T4 per dimer, since each TG dimer
151 contains two sites (one per monomer) of A, B and D and only one Site C.

152 Resolved Sites A, B and D do not show obvious structural similarity and active tyrosines
153 are in solvent accessible and flexible regions (Figure 2a, Extended Data Figure 7a,c). A
154 conserved lysine is found in proximity of the donor, and a conserved acidic residue (Glu
155 or Asp) always precedes the acceptor²¹. By mutagenesis of Site D, we showed that
156 K1415 is not relevant, but D1309 is essential for hormonogenesis (Extended Data
157 Figure 6d). Inserting an additional Ser-Asp sequence before acceptor Y1310 did not
158 change the amount of T4 produced. Therefore, the presence of the aspartate seems to be
159 overall more important than its distance to the donor tyrosine.

160 Because in Sites A, B and D the donor backbone conformation is constrained within
161 secondary structure elements, whereas the acceptor is in more flexible regions, the
162 acidic Asp or Glu residues (pointing towards the solvent) could play a role in orienting
163 the following acceptor towards the more rigid donor. There is no preceding acidic
164 residue in the C-terminal Site C, where both acceptor and donor (Y2766 from the two
165 chains of the dimer) are in unstructured regions with higher intrinsic flexibility.

166 Although the reaction mechanism of T4 synthesis from polypeptide chains remains to
167 be established in more detail, four features seem to be crucial for hormonogenesis:
168 tyrosine pairs must be solvent exposed to be iodinated, in proximity and in roughly
169 antiparallel orientation, and in highly mobile regions of the protein in order to allow the
170 significant bond rearrangement resulting in T4 synthesis.

171 To validate our list of requirements for hormonogenesis from polypeptide chains, we
172 set out to engineer synthetic T4 hormonogenic sites into the unrelated bacterial maltose
173 binding protein (MBP). *E. coli* MBP naturally contains 15 tyrosines, mostly found in its
174 hydrophobic core except the Y171-Y176 pair, which is in a solvent-exposed β -hairpin,
175 and Y341, located in a solvent-exposed helix, facing the C-terminal helix (Extended Data
176 Figure 7b & d). We engineered a putative partner tyrosine for Y341 first via the
177 mutation R367Y (in a neighbouring helix) and second by inserting a tyrosine-containing
178 peptide at the C-terminus: SDYS (C-ins1) or SGSDYS insert (C-ins2). We measured T4
179 hormonogenesis with the same ELISA used for TG (Extended Data Figure 7a), at a
180 concentration corresponding to a single TG site, and 10 times higher, to allow detection
181 of marginal activities (Figure 3b). Unmodified MBP's T4 hormone production was only
182 measurable at the higher concentration. We attribute this basal activity to the
183 Y171/Y176 pair since it could be suppressed by introducing a Y171A mutation. The low
184 level of T4 production can be attributed to a lack of flexibility of the backbone near
185 Y171 and Y176, and to their relative orientations, which is different to any of the sites in
186 TG. Equally, the hormonogenic activity was unchanged when introducing the pair
187 Y341/Y367, presumably because both tyrosines were constrained by their rigid α -
188 helical backbone, and the coupling reaction could not occur with any effectiveness. The
189 C-ins1 variant, producing a putative tyrosine pair with Y341, also showed low activity,
190 possibly because the added linker was designed to be too short for the two tyrosines to
191 come into proximity. However, and significantly, the amount of T4 measured for the
192 two-residue longer C-ins2 MBP variant was comparable to a single site in TG (Figure 3b,
193 Supplementary Video 2). Finally, with our ELISA we could also obtain modest T4
194 synthesis from random tyrosine copolymers, as previously reported⁴ (Extended Data
195 Figure 6e).

196 Nature has selected the complex and large scaffold of the TG dimer to synthesise only
197 seven molecules of hormones, using a chemical reaction involving radicals that could be

198 carried out by unfolded peptides or other less complex proteins. However, in the
199 context of the thyroid gland and the iodine cycle in vertebrates, TG's structure
200 effectively combines hormonogenesis with iodination of many other solvent exposed
201 tyrosine residues for iodine storage^{21,13}. The solvent exposure of tyrosines is
202 presumably compensated by the exceptional solubility and stability that allows TG to
203 persist at high concentrations in the harsh environment of the colloid. Moreover, the
204 complexity of the TG molecule might fulfil further important roles in endocytosis,
205 regulation of the T3/T4 ratio, TG proteolytic processing and in the trafficking to
206 lysosomes^{25,26}. The atomic structure of human TG presented here will enable further
207 studies towards a deeper understanding of thyroglobulin within the thyroid, and its
208 involvement in thyroid diseases^{27,28,29}.

209 **MAIN FIGURE LEGENDS**210 **Figure 1. The structure of human TG by cryo-EM**

211 **a)** Domain assignment of human thyroglobulin. Five regions (NTD, Core, Flap, Arm and
212 CTD) contain domains of type-1 to type-3 TG repeats, as well as the choline esterase-like
213 domain (ChEL), labelled as A to V. **b)** Structural gallery of all resolved TG domains. **c)** TG
214 cryo-EM map where individual subunits are coloured blue and grey. The NTD crosses
215 the major C2 interface. **d)** Ribbon diagram of panel c), coloured as in panel a). **e)**
216 Schematic representation of TG structure in the same colour scheme as in a) and d).

217 **Figure 2. Identification and validation of hormonogenic donor-acceptor tyrosine**
218 **pairs in TG**

219 **a)** Close-up view of the T4 hormonogenic sites resolved in the cryo-EM map, donor and
220 acceptor tyrosines are highlighted in yellow. Site A suggests two donors, Y234 and
221 Y149. **b)** Location of the four hormonogenic Sites A to D in the TG structure. **c)** T4 ELISA
222 after *in vitro* iodination in triplicate. Bar plot and error bars indicate average and
223 standard deviation. Replacing all acceptor tyrosines (Y) with phenylalanines (F)
224 prevents hormone formation (4 Acc: 24, 2573, 2766, 1310). Replacing all five donors
225 suppresses T4 synthesis (4 Donors (1): 2540, 2766, 108, 234; 4 Donors (2): 2540, 2766,
226 108, 149; 5 Donors: 2540, 2766, 108, 234, 149). Replacing other tyrosines at the surface
227 (258, 704, 1467, 1782) has no effect (4eY).

228

229 **Figure 3. Engineering T4 hormone synthesis by bacterial maltose binding protein**
230 **(MBP)**

231 **a)** rTG mutants with only one site active at a time. T4 release measured with the same
232 T4 ELISA as in Figure 2c. The sum of T4 produced by the individual sites recapitulates
233 the T4 produced by WT. **b)** T4 ELISA after *in vitro* iodination of engineered MBP to
234 reconstruct TG's hormonogenic sites. See text and Supplementary Video 2 for details. An
235 MBP version adding a flexible SGSDYS tail to the C-terminus shows activity comparable
236 to a single site on TG as shown in panel a). All measurements done in triplicate. Bar plot
237 and error bars indicate average and standard deviation.

238 **METHODS**239 **DNA constructs**

240 A gene encoding for full length human TG (Uniprot P01266) additionally containing a
241 10x histidine tag at the C-terminus preceded by a TEV cleavage site was codon-
242 optimised for mammalian expression and purchased from GenScript (Piscataway, NJ).
243 The gene was cloned with EcoRI and XhoI restriction sites (enzymes purchased from
244 NEB) into vector pLEXm¹⁴ for recombinant expression in mammalian cells. Mutations
245 were introduced by PCR and the purified overlapping fragments were assembled with
246 the EcoRI/XhoI linearised vector by Gibson assembly (NEB).

247 Maltose binding protein (MBP) constructs were purchased as gBlocks (IDT) and cloned
248 using BlnI and NdeI restriction sites (enzymes purchased from NEB) into the pHis17
249 bacterial vector, for the expression of N-terminally 6x histine-tagged MBP variants. A
250 synthetic gene comprising human TPO (UniProt ID P07202) 1-838 with native
251 extracellular signal sequence was cloned into pFastBac1 plasmid adding a C-terminal 6x
252 histidine tag. All translated sequences of recombinant proteins used in this work are
253 listed in SUPPLEMENTARY INFORMATION 1.

254 **Proteins, protein expression and purification**

255 Endogenous TG (eTG) from human thyroid glands was purchased from Biorad
256 (Hercules, CA). We found it contains some T4, as measured by using our T4-ELISA, but
257 not T3 (Extended Data Figure 6). It is also partially degraded, as shown by SDS-PAGE
258 (Extended Data Figure 2a). While the protein behaved well when performing negative
259 staining EM, it was challenging to produce specimens amenable to high resolution cryo-
260 EM. Therefore, eTG was deglycosylated with the addition of 1 µl/200 µg eTG of PNGaseF
261 from NEB (Ipswich, MA) for 1 h at 37 °C and purified by size exclusion chromatography
262 using a Superose 6 Increase 3.2/300 column (GE Healthcare), equilibrated with buffer
263 T200 (50 mM Tris/HCl, 200 mM NaCl, pH 8.0).

264 For the recombinant production of human TG (rTG), HEK293T (ATCC no. CRL-1573)
265 cells were cultured as adherent monolayers until 90% confluency in Dulbecco's
266 modified Eagle's medium (Sigma-Aldrich Company Ltd., Gillingham, UK) supplemented

267 with 10% foetal calf serum (v/v; Sigma-Aldrich Company Ltd.), L-glutamine and
268 nonessential amino acids (Invitrogen Ltd., Paisley, UK), and transiently transfected with
269 2 mg of DNA and 4 mg of polyethyleneimine (PEI; Sigma-Aldrich Company Ltd.) per litre
270 of culture. We note that the involvement of glycans in TG dimer formation as revealed
271 by the structure might explain the poor expression yields of thyroglobulin when
272 produced in expression systems with reduced/altered glycosylation, such as insect cells,
273 HEK293S GnT1^{-/-} cells or HEK293T cells in the presence of kifunensine (data not
274 shown).

275 Five days later, the supernatant containing approximately 0.5 mg/L of secreted TG was
276 harvested and filtered (0.22 µm) for protein purification. For smaller cultures (~125
277 mL) the supernatant was diluted with an equal volume of buffer T200 containing 20
278 mM imidazole. For volumes larger than 250 mL the supernatant was concentrated and
279 buffer exchanged into buffer T200 using an Äkta Flux system (GE Healthcare).
280 Subsequently, Ni-NTA agarose beads (QIAGEN, West Sussex, UK) were added to the
281 supernatant (2 mL per litre of supernatant). The mixture was gently stirred at 4 °C for 1
282 h and the beads collected by centrifugation at 600 xg for 5 min in 50 mL tubes (Falcon,
283 BD Biosciences, Oxford, UK). The beads were poured into a 10 mL EconoColumn (Bio-
284 Rad Laboratories Ltd., Hemel Hempstead, UK) and washed with 10 column volumes
285 (CV) of buffer T200, supplemented with increasing concentrations of imidazole (20 mM,
286 50 mM, 80 mM), prior to elution with 5 column volumes of buffer T200 supplemented
287 with 500 mM imidazole (all buffers adjusted to pH 8.0). Eluting fractions containing TG,
288 according to SDS-PAGE analysis, were pooled and concentrated prior to further
289 purification by size exclusion chromatography (SEC) using a Superose 6 Increase
290 3.2/300 column (GE Healthcare), or a Superose 6 10/300 GL column for larger amounts
291 of protein. Fractions containing TG were joined, concentrated by ultrafiltration,
292 aliquoted at a concentration of ~0.5 mg/mL, flash frozen in liquid nitrogen and stored at
293 -80 °C.

294 For maltose binding protein (MBP) variants, the plasmid was transformed into
295 chemically competent C41(DE3) *E. coli* cells. 100 mL bacterial cultures were grown in
296 2xTY medium at 37 °C in the presence of 100 µg/mL ampicillin, and protein expression
297 was induced at an optical density OD₆₀₀ of ~1.0 with 1 mM IPTG for 5 hrs. Cells were
298 harvested by centrifugation at 5000 xg, re-suspended in buffer T200, supplemented

299 with 20 mM imidazole, DNase, RNaseA, lysozyme (Sigma Aldrich) and protease
300 inhibitors (Roche), and lysed by sonication. The soluble fraction was separated by
301 ultracentrifugation at 40,000 xg and MBP protein variants were purified as described
302 for TG, with a SEC final purification step using a Superdex 200 3.2/300 column.

303 For human TPO ectodomain expression in insect cells, bacmids were prepared using
304 DH10EMBacY competent cells (Geneva Biotech) following the Bac-to-Bac Baculovirus
305 Expression System user guide by Invitrogen. Sf9 cells were transfected with FuGENE
306 Transfection reagent (Promega). V₁ virus was used for large-scale protein production in
307 400 mL, and cells were supplemented with 5-aminolevulinic acid, which is a precursor
308 of the heme prosthetic group and has been reported to increase specific activity of TPO³⁰.
309 Four days after infection, cells were harvested via centrifugation (800 xg, and then
310 10.000, both at 4 °C) and the supernatant was concentrated by tangential flow filtration.
311 The concentrated supernatant was dialysed against PBS, pH 7.4 and TPO was purified
312 by nickel affinity purification (GE Healthcare HisTrap HP, 1 mL column) using as
313 binding buffer PBS plus 20 mM imidazole, pH 7.4 and as elution buffer PBS plus 400 mM
314 imidazole, also at pH 7.4. Relevant fractions were pooled, concentrated by ultrafiltration
315 and TPO was further purified using a Superdex 200 10/300 column (GE Healthcare),
316 pre-equilibrated with PBS, pH 7.4. TPO was concentrated to 1 mg/mL and flash frozen
317 in liquid nitrogen for storage at -80 °C. The heme occupancy of TPO was estimated by
318 measuring the ratio of absorbance at 412 nm and 280 nm which was 0.2, which roughly
319 equates to 20% occupancy³⁰.

320 **EM sample preparation and data collection**

321 Graphene oxide (GO) grids were prepared following a published procedure³¹ using as
322 support Quantifoil Cu/Rh 200 mesh R2/2 grids. 3 µL of TG sample was applied to the
323 GO grids at a concentration of approximately 0.05 mg/mL and plunge-frozen in liquid
324 ethane using a Vitrobot Mark IV (Thermo Fisher). While eTG behaved better when
325 deglycosylated, there was no difference between glycosylated and deglycosylated rTG.
326 Therefore, we collected datasets of deglycosylated eTG and non-deglycosylated rTG.

327 Images were acquired on a K2 Summit detector (Gatan) in counting mode using a Titan
328 Krios G2 (Thermo Fisher) electron microscope at 300 kV. A Quantum GIF energy filter
329 (Gatan) was used with a slit width of 20 eV to remove inelastically scattered electrons.

330 The eTG dataset was collected at eBIC (Diamond Light Source, UK) while the rTG
331 dataset was collected at MRC-LMB. For the eTG dataset, 40 movie frames were
332 recorded, using a fluency of 1.18 electrons per \AA^2 per frame, for a total accumulated
333 dose of 47.2 electrons per \AA^2 at a pixel size of 1.043 \AA on the specimen. For the rTG
334 dataset 52 movie frames were recorded, using a fluency of 0.91 electrons per \AA^2 per
335 frame, for a total accumulated dose of 36.3 electrons per \AA^2 at a pixel size of 1.149 \AA on
336 the specimen. Further details are presented in Extended Data Table 1.

337 **Cryo-EM image processing**

338 Movie frames were corrected for gain using a reference, motion-corrected and dose-
339 weighted using MOTIONCOR2³². Aligned micrographs were used to estimate the
340 contrast transfer function (CTF) in Gctf³³. All subsequent image-processing steps were
341 performed using single particle reconstruction methods in RELION 2.1 or 3.0^{34,35}. Poor-
342 quality images were discarded after manual inspection. Particles were initially manually
343 picked in order to generate 2D class references for automated picking in RELION. After
344 picking the whole dataset automatically, particles were extracted with 4 x 4 binning and
345 two rounds of reference-free 2D classifications were performed. The particles belonging
346 to the best 2D classes were extracted un-binned (400 pixels box size) and used for 3D
347 reconstruction, applying C2 symmetry. The resolution was estimated with the FSC
348 criterion of 0.143 and B-factor sharpening was applied, both using the
349 `relion_postprocess` routine. Local map resolution was estimated with RELION. Bayesian
350 polishing and per particle CTF and tilt correction were performed but did not provide a
351 significant improvement in resolution.

352 The central regions of the maps, corresponding to the C-terminal ChEL domains, were
353 well defined (~ 3 \AA in resolution), whereas peripheral regions corresponding to the
354 Arms were noisy and at lower resolutions (~ 6 \AA). In order to improve resolution
355 especially in the Arm regions we expanded the dataset using the
356 `relion_symmetry_expand` routine by the C2 symmetry and re-extracted the particles
357 centred at the least resolved part of the map (Extended Data Figure 2d),³⁶. After
358 applying a soft mask to one half of the TG dimer, several cycles of refinement and 3D
359 classification were run using solvent flattening. Although the overall resolution of the
360 expanded and re-centred map was very similar to the C2 counterpart, the local

361 resolution and continuity of the density in the Arm region was significantly improved
362 (Extended Data Figure 2e). The same procedure was applied to both eTG and rTG
363 datasets, which at the end looked virtually identical as shown in Extended Data Figure
364 2g. The best final maps we used for model building were the C2 map from the eTG
365 dataset (overall 3.39 Å resolution) and the expanded map from the rTG dataset (overall
366 3.67 Å resolution). In order to allow simultaneous model building in both maps the
367 expanded rTG map was aligned and resampled onto the C2 map, and subsequently C2
368 symmetrised for the final dimer TG model.

369 **Model building**

370 Following the domain annotations reported in UniprotKB for TG (P01266), we
371 generated homology models with SWISSMODEL³⁷, as reported in Extended Data Table
372 2. We visually inspected the map and localised matching domains for some of the
373 models, which we fitted by correlation in Chimera³⁸. Firstly, the large ChEL domain at
374 the dimeric TG interface was identified; secondly, triplets of TG type-1 repeats were
375 fitted^{16,17}. Their correct order was determined by the differences in side chain densities
376 surrounding the CWC motif and the characteristic loop insertions of each domain. The
377 best resolved type-3 repeat was domain U, which we built *de novo* in MAIN³⁹ and used
378 as a template to generate homology models for the other type-3 repeats Q, R, S and T.
379 The connecting regions with unknown folds were build *de novo* in MAIN³⁹ and COOT⁴⁰,
380 with help of secondary structure predictions (HHpred⁴¹, Jpred⁴²). The correct
381 assignment of the polypeptide chain register was often helped by the presence of large
382 aromatic side chains and disulfide bond pairs, as well as the presence of glycosylation
383 sites at Asn residues (17, plus 4 new sites which we identified, Extended Data Table 3,
384 Extended Data Figure 5a-f). Residues 24 (acceptor Site A) to 29 were built tentatively
385 into a map filtered to lower resolution using MAIN score map density modification
386 procedure³⁹, however their coordinates are only indicative and hence are included in
387 the model as poly-alanine (Extended Data Figure 6g).

388 Initially, the full model was built in one half of the rTG map (expanded, re-centred and
389 masked) and refined using Phenix.real_space_refinement⁴³. Subsequently, the full
390 dimeric structure was generated by applying C2 symmetry and further refined in the
391 C2-symmetrised rTG map. Final statistics and validation of the model are reported in

392 Extended Data Table 1 and Extended Data Figure 2. The resolution of the map is non-
393 uniform and consequently the model has variable quality depending on the map region.
394 To illustrate this, per residue B-factor and per-residue map-to-model cross correlation
395 plots as calculated in Phenix are provided in Extended Data Figure 3.

396 **Crosslinking and mass spectrometry analysis**

397 An rTG aliquot 100 μ L at 0.5 mg/mL was buffer-exchanged using a Superose 6 Increase
398 3.2/300 column (GE Healthcare), pre-equilibrated with 20 mM Hepes, 200 mM NaCl at
399 pH 7.5. Pooled fractions were incubated for 2 h on ice at 0.5 mg/mL with or without 1
400 mM BS³ (bis(sulfosuccinimidyl)suberate, Thermo Fisher). The crosslinking reaction was
401 quenched by adding 50 mM ammonium bicarbonate and the product was analysed
402 using a Superose 6 Increase 3.2/300 column pre-equilibrated in buffer T200 (Extended
403 Data Figure 4). Gel bands corresponding to crosslinked rTG were excised and digested
404 with trypsin (Pierce, Germany) following an in-gel digestion protocol⁴⁴. The resulting
405 tryptic peptides were extracted and desalted using C18 StageTips⁴⁵.

406 Enrichment of crosslinked peptides was accomplished by size-exclusion
407 chromatography using a Superdex Peptide 3.2/300 column (GE Healthcare). Mobile
408 phase consisted of 30% (v/v) acetonitrile and 0.1% trifluoroacetic acid, running at a
409 flow rate of 10 μ L/min. The earliest five peptide-containing fractions (50 μ L each) were
410 collected and dried in a vacuum concentrator.

411 LC-MS/MS analysis was performed using an Orbitrap Fusion Lumos Tribrid mass
412 spectrometer (Thermo Fisher Scientific, Germany), connected to an Ultimate 3000
413 RSLCnano system (Dionex, Thermo Fisher Scientific, Germany). Samples were
414 resuspended in 1.6% v/v acetonitrile 0.1% v/v formic acid and injected onto an EASY-
415 Spray column of 50 cm length (Thermo Fisher) running at 300 nL/min with mobile
416 phases A (0.1% formic acid) and B (80% acetonitrile, 0.1% formic acid). Samples were
417 eluted by applying a gradient ranging from 2% to 45% B over 90 min. Each gradient
418 was optimised for the corresponding SEC fraction. After this, a washing step was
419 applied in which the content of B was ramped to 55% and 95% within 2.5 min each,
420 followed by 5 min at 95% B. Each fraction was analysed in duplicates. The settings of
421 the mass spectrometer were as follows: data-dependent mode with 3s-top-speed
422 setting; MS1 scan in Orbitrap at 120,000 resolution over 400 to 1,600 m/z; MS2-scan

423 trigger only on precursors with $z = 3-6+$; fragmentation by HCD employing a decision
424 tree logic with optimised collision energies; MS2 scan in Orbitrap at resolution of
425 30,000; dynamic exclusion was enabled upon single observation for 60 seconds.
426 Generation of fragment spectra peak lists from raw mass spectrometric data used
427 msConvert (version 3.0.11729), operating under default settings. Precursor m/z were
428 recalibrated and the crosslink search was performed using Xi⁴⁶ using TGs Isoform 1
429 sequence without N-terminal signal peptide sequence and extra residues from TEV-
430 cleavage. Decoy sequences were generated by reversing the protein sequence. For the
431 search MS1 and MS2 accuracies were set to 3 and 10 ppm, respectively. Tryptic peptides
432 (full trypsin specificity) with up to four missed cleavages were allowed. BS³'s reaction
433 specificity was restricted to the side chains of lysine, serine, threonine, tyrosine, as well
434 as the protein N-termini. Carbamidomethylation on cysteine was set as fixed; oxidation
435 on methionine, hydrolysed/aminolysed BS³ from hydrolysis or ammonia quenching on
436 a free cross-linker end were set as variable modifications. Identified crosslinked peptide
437 candidates were filtered to an FDR of 2% on residue-pair-level using XiFDR⁴⁷. A list of all
438 experimental crosslinks is reported in Supplementary Table 1. Inter- and
439 intramolecular theoretical crosslinking pairs were calculated from our TG atomic
440 structure and overlapped with the experimental pairs with a Xi score > 12 and an
441 estimated FDR = 0 (Extended Data Figure 4c).

442

443 **T4 and T3 ELISA**

444 We produced TH from recombinant (non-iodinated) proteins following the procedures
445 reported previously for poorly iodinated eTG²², and quantified the T4 and T3 products
446 via ELISA designed to work in blood serum (Abcam, ab108661: Human Thyroxine
447 ELISA Kit; Abcam, ab108664: Human Triiodothyronine ELISA Kit (free + total T3). To
448 perform the assays, protein at a concentration of 0.1 μM was added to 1 mM KI, 24 mM
449 glucose, 2 $\mu\text{g}/\text{mL}$ glucose oxidase and 3 $\mu\text{g}/\text{mL}$ lactoperoxidase (LPO) or TPO (Extended
450 Data Figure 6c). All commercial reagents were purchased from Sigma. The iodination
451 reaction was allowed to proceed for 10 min at 37 °C and then Pronase protease mix
452 (Roche) was added at $\sim 2.5 \mu\text{g}/\text{mL}$ to digest all enzymes, and TG to release TH. This was
453 followed by heat inactivation for 15 min at 95 °C, a step that does not affect the stability
454 of free T4 or T3⁴⁸. The reaction product was diluted to measure TH production in
455 dynamic range compatible with the ELISA kits. Subsequently, we added BSA at a

456 concentration of 60 mg/mL to the mixture as an essential blocking agent, and added the
457 mixture to ELISA plates for detection, following the manufacturer's instructions. In
458 order to check whether any of the iodination components were interfering with the
459 ELISA (which is optimised for TH detection in serum) we performed the assay without
460 iodide but adding known amounts of T4 or T3 (Sigma Aldrich). This yielded calibration
461 curves similar to the ones provided by the manufacturer, and also showed good
462 dynamic range (Extended Data Figure 6). Only T4 was produced in detectable amounts
463 in our *in vitro* TH production assay. Considering that TG has 3-4 sites, 0.1 μ M was
464 determined to be the optimal starting concentration for the assay. Positive controls
465 were performed with eTG (containing some hormones and partly iodinated) and
466 negative controls with T3 (tri-iodo-thyronine, Sigma), lysozyme and with FtsZ from
467 *Staphylococcus aureus*, which does not contain tyrosines. Using our calibration curve,
468 we converted the absorbance into T4 concentration, performed each measurement
469 three times independently and reported the average and standard deviation values
470 (Extended Data Figure 6, Figures 2 & 3). Recombinant TPO was added at a five times
471 higher concentration, compensating for its heme content of only ~20 %. Tyrosine
472 copolymers were purchased from Sigma Aldrich (P4659, P0151, P4409, P1800) and
473 dissolved in T200 buffer.

474

475 **EXTENDED DATA FIGURE LEGENDS**

476 **Extended Data Figure 1. The iodine cycle in the thyroid gland and the chemistry of**
477 **thyroid hormone formation. a)** Iodide is extracted from the blood vessels and into the
478 thyroid cells via the Na/I symporter (NIS). TSH binds TSH receptor (TSHR) to induce
479 the expression of TG. TG is secreted into the extracellular lumen of follicular cells
480 (colloid). DUOX and TPO catalyse the iodination of TG, therefore T4 (or T3) hormones
481 are formed on the TG polypeptide chain. After hormonogenesis, TG is reimported and
482 proteolysed in lysosomes to release T4/T3 into the blood. DEHAL1 deiodinates iodo-
483 tyrosines to recycle iodide in thyroid cells. **b)** T4 (or T3) synthesis from thyroglobulin
484 (TG) in the thyroid gland.

485

486 **Extended Data Figure 2. Cryo-EM reconstruction of endogenous and recombinant**
487 **thyroglobulin (eTG, rTG).**

488 **a)** SDS-PAGE of endogenous eTG from goitrous thyroid extracts and recombinant rTG
489 expressed in HEK293T cells. **b)** Cryo-EM micrograph of eTG with calculated reference-
490 free 2D class averages below. Scale bar 200 Å. **c)** Cryo-EM micrograph of recombinant
491 rTG with 2D class averages, showing the two proteins to be structurally identical at this
492 level of analysis. Scale bar 200 Å. **d)** Schematic illustrating the C2 symmetry-expansion
493 and re-centring procedure, which was used to enhance TG map quality in peripheral
494 regions. For a detailed procedure see the Methods section 'Cryo-EM image processing'.
495 **e)** Local resolution of the C2 and symmetry-expanded and re-centred eTG maps. **f)**
496 Flexibility of N-terminal domain (NTD) resulting in varying map quality and occupancy
497 of this region in a number of 3D class averages (calculated in RELION). **g)** Fourier shell
498 correlation (FSC) between RELION 'gold standard' half-maps and between the final eTG
499 and rTG maps, showing their strong similarity.

500

501 **Extended Data Figure 3: Local properties of the atomic TG model. a)** Per-residue
502 atomic B-factor and cross correlation with the rTG map, plotted per residue number. **b)**
503 Local B-factor colour-coded onto the surface of the TG structure. **c)** FSC between the
504 map and model calculated for rTG. FSC 0.5 is indicated.

505

506 **Extended Data Figure 4: Validation of TG's three-dimensional architecture by MS**
507 **crosslinking. a)** Size-exclusion chromatograms of rTG before and after BS³ crosslinking
508 and subsequent SDS-PAGE (Coomassie stained). **b)** Negative staining micrograph of
509 crosslinked rTG, showing the absence of higher-order structures caused by unwanted
510 inter-dimer crosslinks. **c)** Plot representing experimental crosslinks (circles)
511 overlapping with predicted crosslinks, calculated from the structure determined here.
512 **d) - f)** Detail of key TG interfaces confirmed by the crosslinking.

513

514 **Extended Data Figure 5: TG cryo-EM map details. a)** All disulfide bonds in TG
515 included in the model (yellow spheres). **b)** Glycans detected in the cryo-EM maps and
516 included in the TG atomic model (green spheres). **c)** Close-up view of a typical alpha
517 helix in the TG cryo-EM map (part of the Core region). **d)** Close-up of a beta sheet in TG
518 (part of the ChEL domain). **e)** Close-up of the disulfide bond C900-C921 (Core region). **f)**
519 Map details of N2013 and N-linked GlcNAc between two TG subunits. **g)** Close-up views
520 showing conformational disorder within the hormonogenic sites, making precise side
521 chain placements difficult, but the backbone positions are resolved (rTG map).

522

523 **Extended Data Figure 6: Quantitative TH ELISA assays. a)** Schematic summarising *in*
524 *vitro* TH synthesis and quantification via ELISA assays. **b)** T4 assay calibration curves
525 with added T4 under manufacturer-recommended and modified (T4 synthesis as
526 performed here) conditions. **c)** Validation of the T4 ELISA assay. eTG presumably
527 contains already reacted tyrosine side chains. rTG produces T4. Addition of iodide is
528 required for the reaction to occur. LPO is as active as TPO, taking the reduced 20%
529 heme content in our TPO into account. Lysozyme (some tyrosines), SaFtsZ (no
530 tyrosines) and T3 produce no T4 signal. **d)** Mutating residues in hormonogenic Site D in
531 a version of TG that is only active in Site D shows that a conserved lysine residue is not
532 important for the reaction. Adding an extra Ser-Asp before Y1310 has no effect, but the
533 mutation D1309S abolished activity. **e)** Synthesis of T4 from tyrosine copolymers as
534 measured by the T4 ELISA assay. Only a polymer where tyrosines are spaced apart and
535 preceded by Lys-Asp produce some T4. Note that activity is lower than in a single site of
536 TG (or MBP, compare with Figure 4). **f)** T3 assay calibration curves with added T3 under

537 recommended and modified (as for T4) conditions. **g)** No significant T3 production was
538 detected from iodinated rTG or eTG from goiter.

539

540 **Extended Data Figure 7: Tyrosine pair proximity plots for TG and MBP. a & b)**

541 Proximity plots of tyrosine residues closer than 15 Å to each other, calculated from TG
542 a) and MBP b) atomic models (TG: this study; MBP PDB ID: 1ANF). The coordinates of
543 each point in the plot represent a tyrosine pair position (residue number). For the TG
544 dimer, the distance between tyrosines from the same or the other subunit in the dimer
545 are shown in grey or black, respectively. In TG there are no more than five pairs that are
546 exposed and in < 15 Å proximity at the same time, predicting the absence of other
547 significant hormonogenic sites. In MBP only one pair closer than 15 Å is sufficiently
548 exposed to be a candidate for hormonogenesis. **c) & d)** Ribbon diagram of TG and MBP
549 where tyrosine residues are represented as spheres and coloured by B-factor, which
550 largely indicates solvent exposed residues.

551

552 **Extended Data Table 1: Thyroglobulin (TG) cryo-EM and model statistics**

553 **Extended Data Table 2: TG domain annotation**

554 **Extended Data Table 3: List of N-linked GlcNac in TG structure**

555

556 ACKNOWLEDGEMENTS

557 We thank Christos Savva, Giuseppe Cannone and Shaoxia Chen (MRC-LMB) for help
558 with electron microscopes. We thank Sjors Scheres, Rafael Fernandez Leiro, Paul
559 Emsley, Viswanathan Chandrasekaran and Simonas Masilius (MRC-LMB) for image
560 processing and model building advice. We acknowledge Radu Aricescu (MRC-LMB) for
561 help with the expression of TG in mammalian cells. Christina Heroven and Duncan
562 Lavery (MRC-LMB) helped with mammalian tissue culture. We thank Frank Bürmann,
563 and Greg Slodkowicz (MRC-LMB) for help with data analysis. Fusinita van den Ent and
564 Tim Nierhaus (MRC-LMB) advised on protein work. We thank Toby Darling and Jake
565 Grimmett (MRC-LMB) for computing support. We thank Dan Clare (eBIC Diamond Light
566 Source) for EM data collection. We acknowledge Diamond Light Source for access and
567 support of the cryo-EM facilities at the UK's National Electron Bio-imaging Centre
568 (eBIC), funded by the Wellcome Trust, MRC and BBRSC. This work was funded by the
569 Medical Research Council (U105184326 to JL), the Wellcome Trust (202754/Z/16/Z to
570 JL, 203149 to JR) and by the Slovenian Research Agency (ARRS; P1-0048, IO-0048 and
571 J1-7479 to DT). This work was supported by the Wellcome Trust through a Senior
572 Research Fellowship (103139 to JR) and by the DFG, German Research Foundation
573 (329673113 and EXC 2008/1 – 390540038 to JR).

574 AUTHOR CONTRIBUTIONS

575 F.C. performed TG mammalian expression, cryo-EM, TG biochemistry, ELISA design and
576 data analysis. F.C., J.L and D.T. built and refined the TG model. A.T.-V. and I.B. performed
577 TPO biochemistry. V.T.C. performed expression of TG in mammalian cells with F.C.. T.I.
578 collected initial negative staining data on eTG. M.R. developed initial eTG purifications.
579 L.S., F.J.O. and J.R. performed crosslinking mass spectrometry analysis. F.C. and J.L.
580 wrote the manuscript. J.L., F.C., D.T. and A.T.-V. were responsible for project strategy
581 and data interpretation.

582

583 AUTHOR INFORMATION STATEMENT

584 Reprints, permissions and materials may be requested from Dusan Turk
585 (dusan.turk@ijs.si) or Jan Löwe (jyl@mrc-lmb.cam.ac.uk). The authors declare no
586 competing interests.

587

588 **DATA AVAILABILITY STATEMENT**

589 Datasets generated during the current study are available on the following
590 repositories: PDB ID: 6SCJ; EMDB: EMD-10141; ProteomeXchange: PXD014821. All
591 other data generated or analysed during this study are included in this published article (and
592 its supplementary information files).

593

594

595

596 **References**

- 597 1. Di Jeso, B. & Arvan, P. Thyroglobulin From Molecular and Cellular Biology to Clinical
598 Endocrinology. *Endocr. Rev.* **37**, 2–36 (2016).
- 599 2. Citterio, C. E., Targovnik, H. M. & Arvan, P. The role of thyroglobulin in thyroid
600 hormonogenesis. *Nat. Rev. Endocrinol.* **15**, 323–338 (2019).
- 601 3. Carvalho, D. P. & Dupuy, C. Thyroid hormone biosynthesis and release. *Mol. Cell.*
602 *Endocrinol.* **458**, 6–15 (2017).
- 603 4. Cahnmann, H. J., Pommier, J. & Nunez, J. Spatial requirement for coupling of
604 iodotyrosine residues to form thyroid hormones. *Proc. Natl. Acad. Sci. U. S. A.* **74**, 5333–
605 5335 (1977).
- 606 5. Holzer, G. *et al.* Thyroglobulin Represents a Novel Molecular Architecture of Vertebrates.
607 *J. Biol. Chem.* **291**, 16553–16566 (2016).
- 608 6. Taylor, P. N. *et al.* Global epidemiology of hyperthyroidism and hypothyroidism. *Nat.*
609 *Rev. Endocrinol.* **14**, 301–316 (2018).
- 610 7. Sellitti, D. F. & Suzuki, K. Intrinsic Regulation of Thyroid Function by Thyroglobulin.
611 *Thyroid* **24**, 14 (2014).
- 612 8. Xiao, S., Dorris, M. L., Rawitch, A. B. & Taurog, A. Selectivity in tyrosyl iodination sites
613 in human thyroglobulin. *Arch. Biochem. Biophys.* **334**, 284–294 (1996).
- 614 9. Heidelberger, M. The molecular weight of thyroglobulin. *Science* **80**, 414 (1934).
- 615 10. Gavaret, J.M., Cahnmann, H.J., Nunez, J. Thyroid Hormone Synthesis in Thyroglobulin.
616 *J. Biol. Chem.* **256**, 9167–9173 (1981).
- 617 11. Mondal, S., Raja, K., Schweizer, U. & Muges, G. Chemistry and Biology in the
618 Biosynthesis and Action of Thyroid Hormones. *Angew. Chem. Int. Ed.* **55**, 7606–7630
619 (2016).
- 620 12. Gnidehou, S. *et al.* Iodotyrosine dehalogenase 1 (DEHAL1) is a transmembrane protein
621 involved in the recycling of iodide close to the thyroglobulin iodination site. *FASEB J. Off.*
622 *Publ. Fed. Am. Soc. Exp. Biol.* **18**, 1574–1576 (2004).
- 623 13. Dedieu, A., Gaillard, J.-C., Pourcher, T., Darrouzet, E. & Armengaud, J. Revisiting
624 iodination sites in thyroglobulin with an organ-oriented shotgun strategy. *J. Biol. Chem.*
625 **286**, 259–269 (2011).
- 626 14. Aricescu, A. R., Lu, W. & Jones, E. Y. A time- and cost-efficient system for high-level
627 protein production in mammalian cells. *Acta Crystallogr. D Biol. Crystallogr.* **62**, 1243–
628 1250 (2006).
- 629 15. Berg, G., Björkman, U. & Ekholm, R. The structure of newly synthesized intracellular
630 thyroglobulin molecules. *Mol. Cell. Endocrinol.* **20**, 87–98 (1980).
- 631 16. Gunčar, G., Pungerčič, G., Klemenčič, I., Turk, V. & Turk, D. Crystal structure of MHC
632 class II-associated p41 Ii fragment bound to cathepsin L reveals the structural basis for
633 differentiation between cathepsins L and S. *EMBO J.* **18**, 793–803 (1999).
- 634 17. Molina, F., Bouanani, M., Pau, B. & Granier, C. Characterization of the Type-1 Repeat
635 from Thyroglobulin, a Cysteine-Rich Module Found in Proteins from Different Families.
636 *Eur. J. Biochem.* **240**, 125–133 (1996).

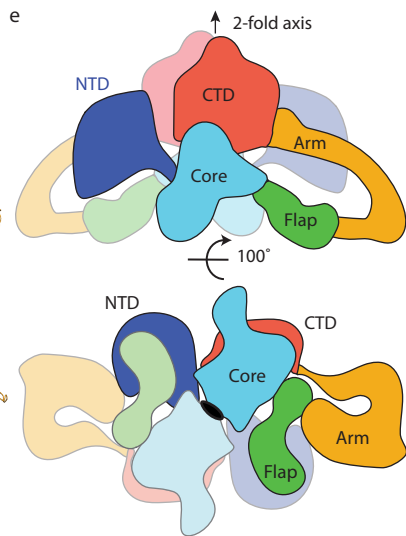
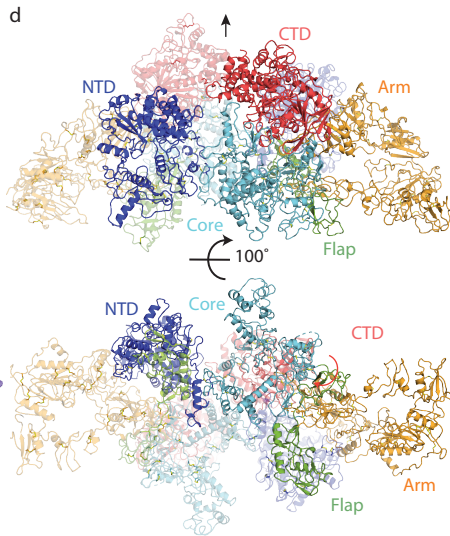
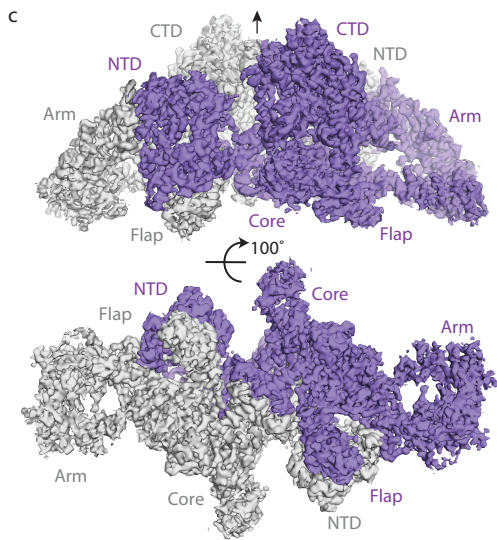
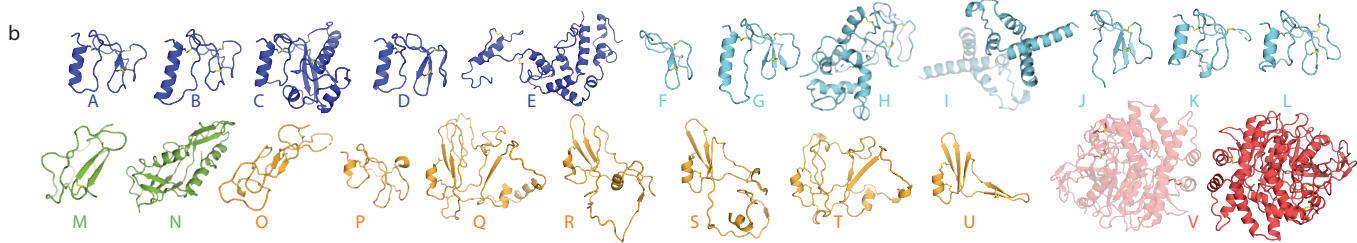
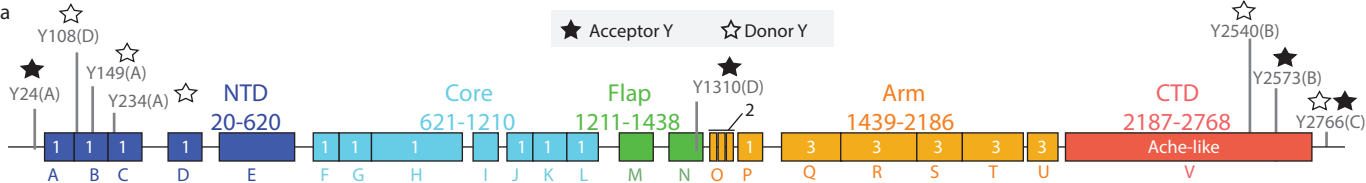
- 637 18. Lee, J. & Arvan, P. Repeat motif-containing regions within thyroglobulin. *J. Biol.*
638 *Chem.* **286**, 26327–26333 (2011).
- 639 19. Citterio, C. E., Morishita, Y., Dakka, N., Veluswamy, B. & Arvan, P. Relationship
640 between the dimerization of thyroglobulin and its ability to form triiodothyronine. *J. Biol.*
641 *Chem.* **293**, 4860–4869 (2018).
- 642 20. Yang, S.-X., Pollock, H. G. & Rawitch, A. B. Glycosylation in Human Thyroglobulin:
643 Location of the N-Linked Oligosaccharide Units and Comparison with Bovine
644 Thyroglobulin. *Arch. Biochem. Biophys.* **327**, 61–70 (1996).
- 645 21. Lamas, L., Anderson, Peggy C., Foxy, Jay W. & Dunn, John T. Consensus Sequences
646 for Early Iodination and Hormonogenesis in Human Thyroglobulin. *J. Biol. Chem.* **264**, 5
647 (1989).
- 648 22. Pommier, J., Deme, D. & Nunez, J. Effect of Iodide Concentration on Thyroxine
649 Synthesis Catalysed by Thyroid Peroxidase. *Eur. J. Biochem.* **37**, 406–414 (1973).
- 650 23. de Vijlder, J. & den Hartog, M. Anionic iodotyrosine residues are required for
651 iodothyronine synthesis. *Eur. J. Endocrinol.* **138**, 227–231 (1998).
- 652 24. Dunn, J., Kim, PS & Dunn AD. Favored Sites for Thyroid Hormone Formation on the
653 Peptide Chains of Human Thyroglobulin. *J. Biol. Chem.* **257**, 88–94 (1982).
- 654 25. Botta, R. *et al.* Sortilin is a putative postendocytic receptor of thyroglobulin.
655 *Endocrinology* **150**, 509–518 (2009).
- 656 26. Weber, J. *et al.* Interdependence of thyroglobulin processing and thyroid hormone
657 export in the mouse thyroid gland. *Eur. J. Cell Biol.* **96**, 440–456 (2017).
- 658 27. Rivolta, C. M. & Targovnik, H. M. Molecular advances in thyroglobulin disorders. *Clin.*
659 *Chim. Acta* **374**, 8–24 (2006).
- 660 28. Latrofa, F. *et al.* Thyroglobulin autoantibodies in patients with papillary thyroid
661 carcinoma: comparison of different assays and evaluation of causes of discrepancies. *J.*
662 *Clin. Endocrinol. Metab.* **97**, 3974–3982 (2012).
- 663 29. Fiore, E., Latrofa, F. & Vitti, P. Iodine, thyroid autoimmunity and cancer. *Eur. Thyroid*
664 *J.* **4**, 26–35 (2015).
- 665
- 666

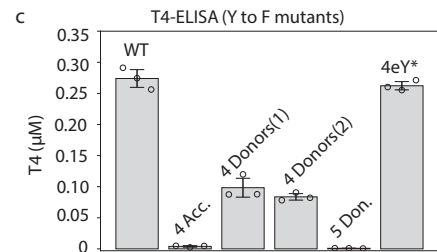
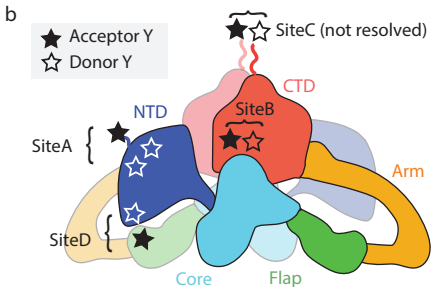
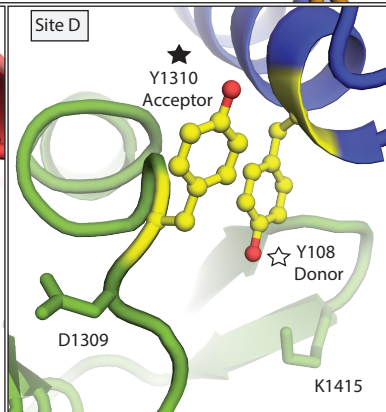
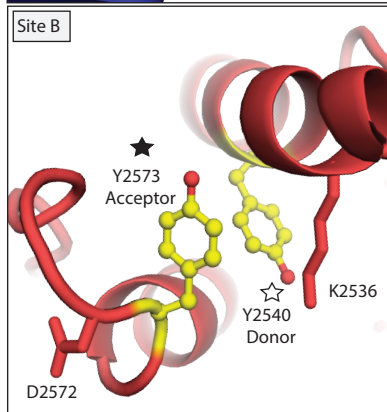
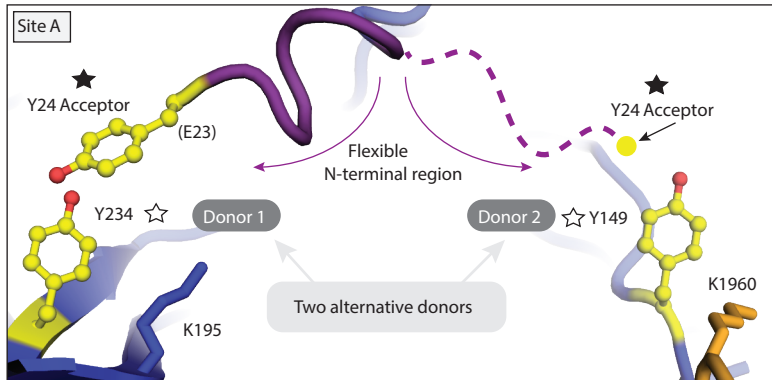
667 **METHODS REFERENCES**

668

- 669 30. Guo, J., Mclachlan, S. M., Hutchison, S. & Rapoport, B. The Greater Glycan Content of
670 Recombinant Human Thyroid Peroxidase of Mammalian Than of Insect Cell Origin
671 Facilitates Purification to Homogeneity of Enzymatically Protein Remaining Soluble at
672 High Concentration. *Endocrinology* **139**, 7 (1998).
- 673 31. Bokori-Brown, M. *et al.* Cryo-EM structure of lysenin pore elucidates membrane
674 insertion by an aerolysin family protein. *Nat. Commun.* **7**, 11293 (2016).
- 675 32. Zheng, S. Q. *et al.* MotionCor2 - anisotropic correction of beam-induced motion for
676 improved cryo-electron microscopy. *Nat. Methods* **14**, 331–332 (2017).
- 677 33. Zhang, K. Gctf: Real-time CTF determination and correction. *J. Struct. Biol.* **193**, 1–12
678 (2016).
- 679 34. Scheres, S. H. W. RELION: Implementation of a Bayesian approach to cryo-EM
680 structure determination. *J. Struct. Biol.* **180**, 519–530 (2012).
- 681 35. Zivanov, J. *et al.* New tools for automated high-resolution cryo-EM structure
682 determination in RELION-3. *eLife* **7**, e42166 (2018).
- 683 36. Li, Y. *et al.* Mechanistic insights into caspase-9 activation by the structure of the
684 apoptosome holoenzyme. *Proc. Natl. Acad. Sci.* **114**, 1542–1547 (2017).
- 685 37. Waterhouse, A. *et al.* SWISS-MODEL: homology modelling of protein structures and
686 complexes. *Nucleic Acids Res.* **46**, W296–W303 (2018).
- 687 38. Pettersen, E. F. *et al.* UCSF Chimera--a visualization system for exploratory research
688 and analysis. *J. Comput. Chem.* **25**, 1605–1612 (2004).
- 689 39. Turk, D. MAIN software for density averaging, model building, structure refinement
690 and validation. *Acta Crystallogr. D Biol. Crystallogr.* **69**, 1342–1357 (2013).
- 691 40. Emsley, P. & Cowtan, K. Coot: model-building tools for molecular graphics. *Acta*
692 *Crystallogr. D Biol. Crystallogr.* **60**, 2126–2132 (2004).
- 693 41. Söding, J., Biegert, A. & Lupas, A. N. The HHpred interactive server for protein
694 homology detection and structure prediction. *Nucleic Acids Res.* **33**, W244–W248 (2005).
- 695 42. Drozdetskiy, A., Cole, C., Procter, J. & Barton, G. J. JPred4: a protein secondary
696 structure prediction server. *Nucleic Acids Res.* **43**, W389–W394 (2015).
- 697 43. Afonine, P. V. *et al.* Real-space refinement in PHENIX for cryo-EM and
698 crystallography. *Acta Crystallogr. Sect. Struct. Biol.* **74**, 531–544 (2018).
- 699 44. Shevchenko, A., Tomas, H., Havli, J., Olsen, J. V. & Mann, M. In-gel digestion for
700 mass spectrometric characterization of proteins and proteomes. *Nat. Protoc.* **1**, 2856–2860
701 (2006).
- 702 45. Rappsilber, J., Ishihama, Y. & Mann, M. Stop and go extraction tips for matrix-assisted
703 laser desorption/ionization, nanoelectrospray, and LC/MS sample pretreatment in
704 proteomics. *Anal. Chem.* **75**, 663–670 (2003).
- 705 46. Mendes, M. L. *et al.* An integrated workflow for crosslinking mass spectrometry.
706 <http://biorxiv.org/lookup/doi/10.1101/355396> (2018) doi:10.1101/355396.
- 707 47. Fischer, L. & Rappsilber, J. Quirks of Error Estimation in Cross-Linking/Mass
708 Spectrometry. *Anal. Chem.* **89**, 3829–3833 (2017).

- 709 48. Ledeti, I. *et al.* Thermal stability of synthetic thyroid hormone l-thyroxine and l-
710 thyroxine sodium salt hydrate both pure and in pharmaceutical formulations. *J. Pharm.*
711 *Biomed. Anal.* **125**, 33–40 (2016).
712

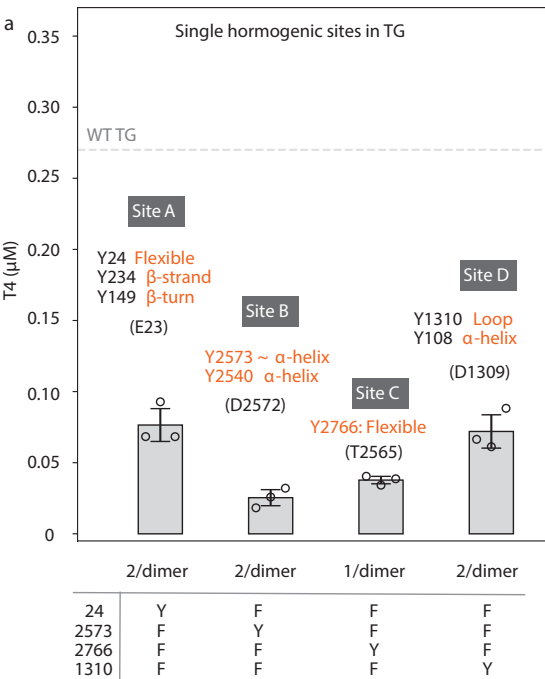




Site A	★ 24	F	Y	Y	Y	Y
	☆ 149	Y	Y	F	F	Y
	☆ 234	Y	F	Y	F	Y
Site B	★ 2573	F	Y	Y	Y	Y
	☆ 2540	Y	F	F	F	Y
Site C	★ 2766	F	F	F	F	Y
	☆ 2766	F	F	F	F	Y
Site D	★ 1310	F	Y	Y	Y	Y
	☆ 108	Y	F	F	F	Y

*4eY = 4 other exposed Y: 258, 704, 1467, 1782

a



b

